Research Article Vol. 30, No. 8 / 11 Apr 2022 / Optics Express 13616
Optics EXPRESS

Design of the all-silicon long-wavelength infrared achromatic metalens based on deep silicon etching

DONGZHI SHAN,[1,2] NIANXI XU,[1] JINSONG GAO,[1,2,*] NAITAO SONG,[1] HAI LIU,[1] YANG TANG,[1] XIAOGUO FENG,[1] YANSONG WANG,[1] YI ZHAO,[1] XIN CHEN,[1] AND QIAO SUN[1]

[1] *Key Laboratory of Optical System Advanced Manufacturing Technology, Changchun Institute of Optics, Fine Mechanics and Physics, Chinese Academy of Sciences, Changchun 130033, China*
[2] *University of the Chinese Academy of Sciences, Beijing 100039, China*
[*] *gaojs999@163.com*

Abstract: An all-silicon long-wavelength infrared (LWIR) achromatic metalens based on deep silicon etching is designed in this paper. With a fixed aperture size, the value range of the equivalent optical thickness of the non-dispersive meta-atoms constructing the achromatic metalens determines the minimum f-number. The fabrication characteristic with high aspect ratio of deep silicon etching amplifies the difference value of optical thickness between different meta-atoms by increasing the propagation distance of the propagation mode, which ensures a small f-number to obtain a better imaging resolution. A 280-μm-diameter silicon achromatic metalens with a f-number of 1 and the average focusing efficiency of 27.66% has been designed and simulated to validate the feasibility of this strategy. The simulation results show that the maximum focal length deviation percentage from the target value between the wavelength of 8.6 and 11.4 μm is 1.61%. This achromatic metalens design is expected to play a role in the field of LWIR integrated optical system.

1. Introduction

The long-wavelength infrared (LWIR) thermal imaging technology plays a more and more important role in many areas, such as medical diagnosis, facilities maintenance and environmental monitoring [1], and the LWIR lens is the core device in the imaging system. However, the traditional refractive optical lens usually possesses the characteristics of bulky volume and curved surface due to the method of the wavefront modulation depending on the change of the optical thickness distribution along the optical path [2]. These features will not only introduce spherical aberration into the imaging system, but also will not be conducive to satisfy the integrated and lightweight assembly requirements [3]. Therefore, the LWIR imaging element which owns simple fabricating process and can be easily integrated has always been an attractive research field.

Metasurface, a two-dimensional planar thin layer structure which is composed of the subwavelength electromagnetic scatterers, attracts more and more attention due to its ability to modulate the wavefront in sub-wavelength scale [4–9]. Many promising achievements have emerged, such as metalens [10,11], beam deflectors and splitters [12,13], holograms [14,15] and vortex beam generators [16,17]. Among them, the metalens is expected to become a new choice in the integrated optical system because it circumvents many limitations existing in the refractive optical elements [18]. The research of the achromatic metalens is of great significance for wide band imaging, and some excellent research results have emerged in visible or near-infrared band [19–22]. However, the researches of the achromatic metalens aiming at the long-wavelength

#449870 https://doi.org/10.1364/OE.449870
Journal © 2022 Received 29 Nov 2021; revised 26 Feb 2022; accepted 28 Mar 2022; published 7 Apr 2022

Optics EXPRESS

infrared are of a relatively small number, and some realizable design methods need further exploration.

In this paper, we design a LWIR achromatic metalens consisting of the all-silicon meta-atoms with high aspect ratio based on deep silicon etching. First, we deduce the design constraint of the achromatic metalens after analyzing the cause of the chromatic aberration of the diffractive metalens. Then, the significance of adopting the all-silicon meta-atoms with high aspect ratio is discussed since the value range of the equivalent optical thickness of the non-dispersive meta-atoms constructing the achromatic metalens determines the minimum f-number with a fixed aperture size. Finally, we simulate a LWIR achromatic metalens whose diameter is 280 μm and f-number is 1 to validate the feasibility of this strategy, and the maximum focal length deviation percentage from the target value between the wavelength of 8.6 and 11.4 μm is 1.61%. In contrast, the maximum focal length deviation percentage of the diffractive metalens with the same aperture, the same material and the same f-number is 15.0%.

2. Design

Different from the refractive lens, the chromatic aberration of the LWIR metalens based on the diffraction focusing effect mainly comes from diffraction effect rather than the wavelength dispersion of the optical materials [23–26]. The reason for this phenomenon is that the diffractive metalens selects the building elements with the same structural parameters to satisfy the same phase requirement at different positions on the aperture [24]. The required phase at position r must satisfy the following equation [27]:

$$\varphi = -\frac{2\pi}{\lambda}\left(\sqrt{r^2 + f^2} - f\right) + 2m\pi, m = 0, 1, 2... \tag{1}$$

where λ is the target wavelength, f is the focal length and the value range of φ is $0\sim-2\pi$. Figure 1(b) shows the structure characteristics of the diffractive metalens, and the elements of the same color are with the same structural parameters. As shown in Fig. 1(b), the metasurface element distribution of the diffractive metalens has spatial repeatability. To the target wavelength λ, the diffractive metalens selects the same metasurface elements to satisfy the same phase requirement on different diffraction rings, and this modeling method leads to the result that the structure of diffractive metalens is similar to the binary optical lens [28]. Figure 1(c) and Fig. 1(d) show the change of the phase distribution curves at different wavelengths to a fixed f-number, and the phase difference between two fixed positions on the metalens aperture varies with wavelength. Obviously, the diffractive metalens cannot meet the phase change requirement shown in Fig. 1(d), and its wavelength dispersion property is similar to that of the diffractive elements.

In order to illustrate the chromatic aberration of the diffractive metalens, silicon is selected as the base material of the metalens to eliminate the influence of material dispersion, whose refractive index changes very little in a broad LWIR bandwidth from wavelength of 8.5 μm to 10.5 μm [29]. The isolated cylindrical waveguide model is chosen to work as the basic element model to construct the metalens as shown in Fig. 2(a) [27]. The period and height of these cylinder nanopillars is 5 μm and 6 μm respectively, and the diameter varies from 1 μm to 3 μm. The simulations are performed using the finite-difference-time-domain (FDTD) method with plane wave illumination from substrate for an infinitely periodic array of these cylinder nanopillars. The simulated amplitude and phase distribution are shown in Fig. 2(c) and Fig. 2(d). Generally, eight basic building elements are selected by uniform discretizing 2π phase to construct the metalens for simplicity, and the diffraction efficiency can reach 95% according to this modeling method [28]. The eight building elements which we have chosen are shown in Fig. 2(b), and the target wavelength is 9.5 μm.

Based on the eight selected elements in Fig. 2(b), we simulate the focusing property of the diffractive metalens with different aperture sizes at the same f-number. The variation results of

Optics EXPRESS

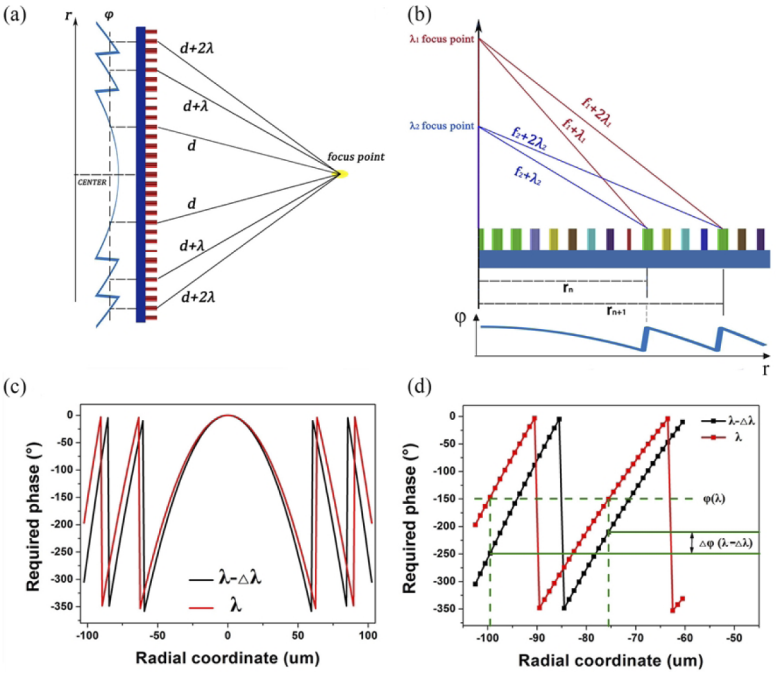

Fig. 1. (a) The schematic diagram of the metalens focusing effect. (b) The structural diagram of the diffractive metalens. Here, the elements of the same color have the same structural parameters. (c) The schematic diagram of the change of phase distribution curve of the metalens with wavelength. (d) Part of the enlarged drawing of the change of phase distribution curve of the metalens with wavelength.

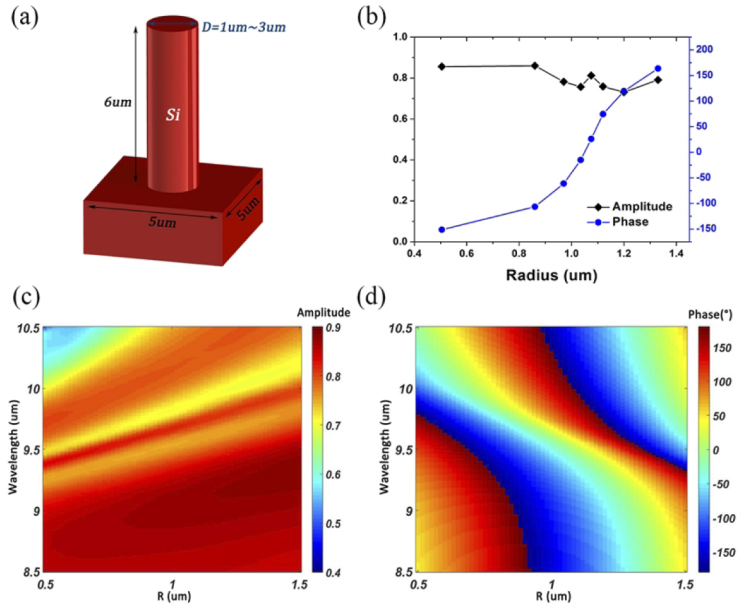

Fig. 2. (a) The schematic diagram of the cylinder nanopillars. (b) Simulated amplitude and phase of the eight selected nanopillars at the target wavelength. (c) The simulated transmission amplitude distribution of the cylinder nanopillars. (d) The simulated transmission phase distribution of the cylinder nanopillars.

Optics EXPRESS

focal length with wavelength are shown in Fig. 3. For the ideal diffractive lenses, the product of the working wavelength and the focal length is a fixed value, as described in the Eq. (2) [30]:

$$f_1 \cdot \lambda_1 = f_2 \cdot \lambda_2 = \ldots = f_n \cdot \lambda_n \tag{2}$$

where $[\lambda_1, \lambda_2 \ldots \lambda_n]$ is the working wavelength range and $[f_1, f_2 \ldots f_n]$ is the corresponding focal length range. The variation of the theoretical focal length values in Fig. 3 follows Eq. (2). With the increase of the number of diffraction rings, the FDTD simulation result is gradually approaching the theoretical value, which shows that the diffractive metalens has obvious diffractive lens property and severe chromatic aberration.

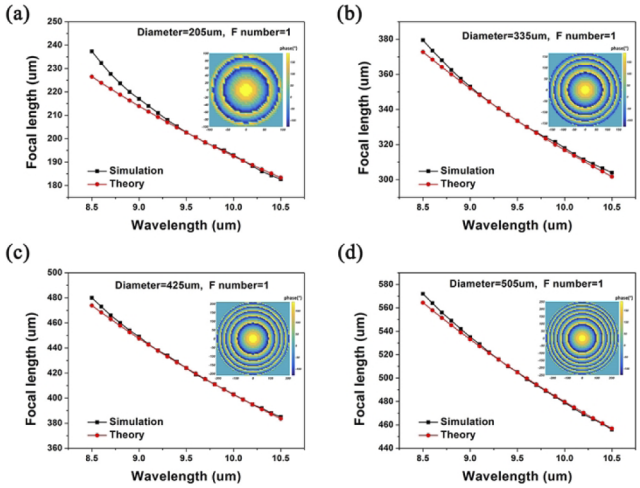

Fig. 3. The schematic diagram of variation of focal length of the diffractive metalens with wavelength. (a) Diameter = 205μm, f-number = 1. (b) Diameter = 335μm, f-number = 1. (c) Diameter = 425μm, f-number = 1. (d) Diameter = 505μm, f-number = 1.

The phase shift φ of the electromagnetic wave through the meta-atom can be simplified as [27]:

$$\varphi = n_{eff} h \frac{2\pi}{\lambda} \tag{3}$$

where λ is the working wavelength, n_{eff} is the equivalent refractive index of the propagation mode of the meta-atom and h is the height of the meta-atom, i.e. the propagation distance of the propagation mode. By substituting Eq. (3) into Eq. (1), the following equation can be obtained:

$$\varphi(r, \lambda) - \varphi(0, \lambda) = n_{eff}(r, \lambda) h(r) \frac{2\pi}{\lambda} - n_{eff}(0, \lambda) h(0) \frac{2\pi}{\lambda} \tag{4}$$

$$n_{eff}(r, \lambda) h(r) \frac{2\pi}{\lambda} - n_{eff}(0, \lambda) h(0) \frac{2\pi}{\lambda} = -\frac{2\pi}{\lambda} (\sqrt{r^2 + f^2} - f) \tag{5}$$

where $\varphi\ (r,\ \lambda)$ and $\varphi\ (0,\ \lambda)$ represent the required phase at the position r and the metalens center to the wavelength λ respectively, and $n_{eff}\ (r,\ \lambda)$ and $n_{eff}\ (0,\ \lambda)$ represent the required equivalent refractive index of the meta-atom at the position r and the metalens center to the wavelength λ respectively. Assuming that through appropriate design, the equivalent refractive index of the meta-atom does not vary with wavelength, and the height of the meta-atoms is consistent.

Optics EXPRESS

Equation (5) can be further expressed as:

$$n_{eff}(r) = n_{eff}(0) - \frac{1}{h}(\sqrt{r^2 + f^2} - f) \tag{6}$$

It can be seen from Eq. (6) that the distribution of equivalent refractive index is independent of the wavelength. For a metalens with diameter D, the same focal length value under different wavelength has the same requirement of the equivalent refractive index distribution. Conversely, on the premise that the equivalent refractive index of the meta-atom does not change with the wavelength, the metalens model designed according to the equivalent refractive index distribution requirement of λ_1 in the working wavelength band naturally satisfies the equivalent refractive index distribution requirement of other wavelengths in the working wavelength band. Equation (6) is equivalent to Eq. (1) on the premise that the meta-atoms are zero-dispersion. Therefore, from the perspective of equivalent refractive index, meta-atoms constituting the achromatic metalens should be distributed according to Eq. (6), and a suitable wavelength should be selected and substituted into Eq. (1) as the boundary condition. The combination of Eq. (6) and Eq. (1) gives the constraints of designing the achromatic metalens, as described below:

$$\begin{cases} n_{eff}(r) = n_{eff}(0) - \frac{1}{h}(\sqrt{r^2 + f^2} - f) \\ \varphi(r) = -\frac{2\pi}{\lambda_t}(\sqrt{r^2 + f^2} - f) + 2m\pi, m = 0, 1, 2 \ldots \end{cases} \tag{7}$$

where λ_t is the selected target wavelength and n_{eff} is the equivalent refractive index of the meta-atoms in the working wavelength band. The achromatic focusing process of the metalens designed according to Eq. (7) is described in Fig. 4.

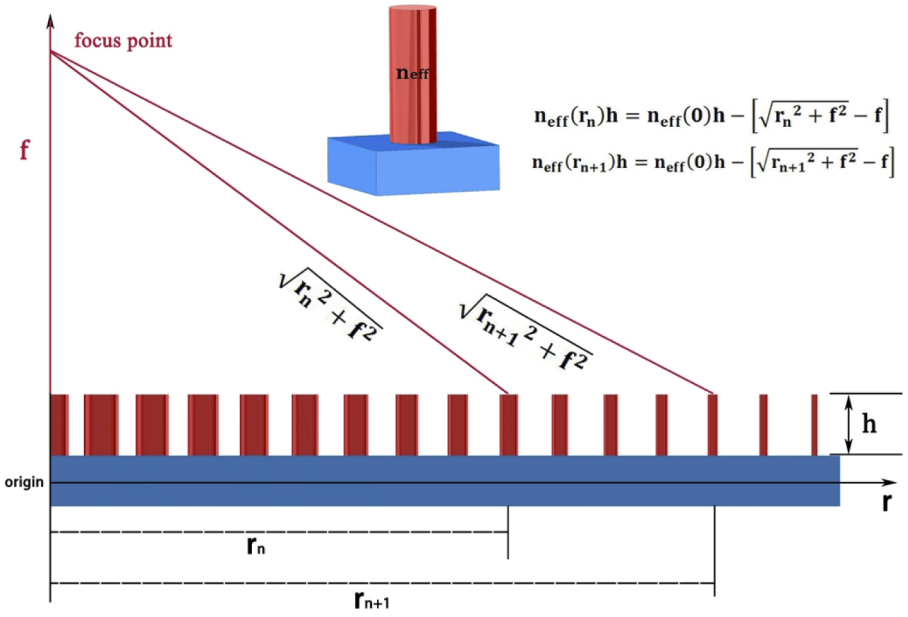

Fig. 4. The schematic diagram of the achromatic metalens focusing effect.

Equation (6) can also be written as follows:

$$r_{\max} = \frac{\triangle n_{eff} h}{\sqrt{1 + 4F^{\#2}} - 2F^{\#}} \tag{8}$$

Optics EXPRESS

where r_{max} is the metalens radius, $F^{\#}$ is the f-number of the metalens, h is the height of the meta-atoms and $\bigtriangleup n_{eff}$ represents the maximum equivalent refractive index difference value among the meta-atoms. Equation (8) shows the relationship between f-number of the metalens and the value range of the equivalent optical thickness of the non-dispersive meta-atoms constructing the achromatic metalens, as shown in Fig. 5. In general, the long-wavelength infrared imaging systems require a small f-number. Therefore, increasing the value range of the equivalent optical thickness of the meta-atoms is of great significance to improve the imaging performance. There are mainly the following two ways to achieve this goal, (a) increasing the value range of the equivalent refractive index n_{eff}, and (b) increasing the value of the height of the meta-atoms h.

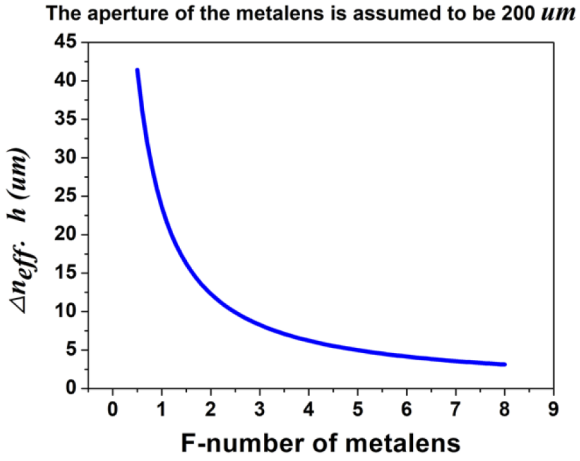

Fig. 5. The relationship diagram between f-number of the metalens and the value range of the equivalent optical thickness of the non-dispersive meta-atoms constructing the achromatic metalens, with the aperture of the metalens assumed to be 200 μm.

The value range of the equivalent refractive index of the propagation mode of the meta-atoms is limited by the refractive index of the optical materials [20], and increasing the structural complexity of the meta-atoms cannot significantly increase the value range of the equivalent refractive index, but greatly increases fabrication difficulty.

In contrast, increasing the aspect ratio of the structure of the meta-atoms instead of increasing the complexity of the structure can linearly broaden the value range of the equivalent optical thickness. The fabrication technology corresponding to this method is required to possess the characteristics of high aspect ratio and straight side-wall to ensure that the propagation mode accumulates the optical thickness in the propagation direction. Deep silicon etching technology has the fabrication characteristics of high aspect ratio and straight side-wall [31,32], which is consistent with the above requirements. Therefore, combined with the fabrication characteristics of deep silicon etching, the achromatic design is carried out by selecting all-silicon blocks coupled waveguide structure with large aspect ratio to construct the metalens. This strategy will extend the design possibility of the achromatic metalens.

3. Simulation experiments

We choose the coupled waveguides model as the building element model to construct the achromatic metalens, which possesses the ability to tailor the dispersion behavior of silicon nanophotonic slot waveguides [33–35]. Figure 6 shows the schematic diagram of the meta-atoms. The material of the metalens is silicon, and due to the proposed deep silicon etching technology, the simulation design is carried out on the premise that the structure has a high aspect ratio [31,32].

Optics EXPRESS

The parameters of our simulation experiment are as follows: the height h of the meta-atoms is 20 μm, the period P of the meta-atoms is 5 μm, the space g between two waveguides is 0.5 μm, the parameter L1 sweeps from 2.6 to 4.0 μm in steps of 0.1 μm, the parameter W1 sweeps from 0.6 to 1.0 μm in steps of 0.1 μm, the parameter L2 sweeps from 1.6 to 3.0 μm in steps of 0.1 μm, the parameter W2 sweeps from 1.1 to 1.5 μm in steps of 0.1 μm, and simulation wavelength range is 9~11 μm.

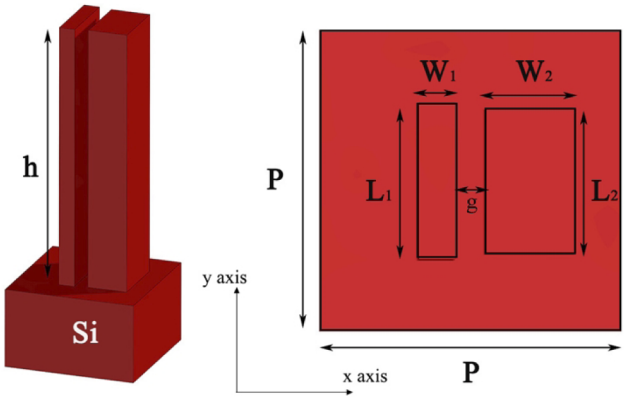

Fig. 6. The schematic diagram of the coupled waveguide model meta-atoms.

We choose circular polarization as the polarization mode of the incident electromagnetic wave, and analyze the cross-polarization response of the meta-atoms. In this way, Pancharatnam-Berry (P-B) phase can be introduced into the design, and it will help to adjust the initial phase of the meta-atoms by rotating the element around its center [36–39]. The electromagnetic response of the meta-atoms excited by a circular polarization incident wave can be expressed by the Jones vector [40]:

$$\begin{bmatrix} \widetilde{E}_x \\ \widetilde{E}_y \end{bmatrix} = \frac{\widetilde{t}_x + \widetilde{t}_y}{2} \begin{bmatrix} 1 \\ \mp i \end{bmatrix} + \frac{\widetilde{t}_x - \widetilde{t}_y}{2} e^{\mp i2\alpha} \begin{bmatrix} 1 \\ \pm i \end{bmatrix} \tag{9}$$

where $\tilde{t}_x$ and $\tilde{t}_y$ represent complex transmission coefficients when the normalized electric field of the incident electromagnetic wave is polarized along the x and y axis of the meta-atoms, and the α term is defined as the counterclockwise rotation angle of meta-atoms with respect to the y-axis.

By sweeping the structural parameters, the equivalent refractive index of the meta-atoms corresponding to the cross-polarization mode excited by the circular polarization electromagnetic wave can be calculated by the following equation.

$$n_{eff} = \frac{\partial \varphi}{\partial(\frac{2\pi}{\lambda})} \frac{1}{h} \tag{10}$$

In order to satisfy the wavelength non-dispersion property of the meta-atoms, we specify that the elements whose coefficient of determination of the linear fitting curve of P-B phase varying with wave number is greater than 0.985 can be adopted to construct the achromatic metalens. Finally, we obtain the meta-atoms group with the cross-polarization equivalent refractive index between 2.2190 and 3.7543. The dispersion curves and electric field distribution of cross-polarization of 4 meta-atoms with different structural parameters are shown in Fig. 7, the structural parameters are shown in Table 1, and the green shaded area in the figures corresponds to the design wavelength band from 9 μm to 11 μm. Through comparison, it can be seen that the coupled waveguide model can tailor the interaction relationship of different modes without increasing the complexity of the cross-section structure to change the equivalent refractive index of the meta-atoms.

Optics EXPRESS

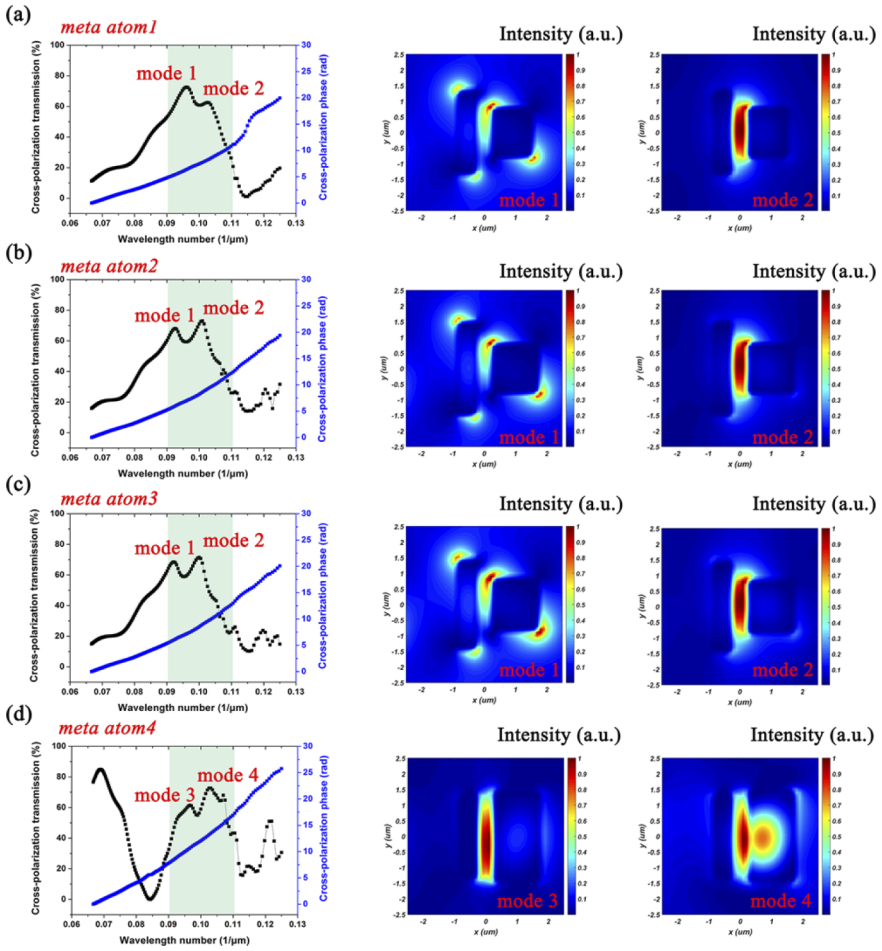

Fig. 7. The dispersion curves and electric field distribution of cross-polarization of the meta-atoms with different structural parameters.

Table 1. The Structural Parameters and Cross-polarization Equivalent Refractive Index n_{eff} of the Meta-atoms in Fig. 7

No.	L_1 (μm)	W_1 (μm)	L_2 (μm)	W_2 (μm)	Period (μm)	Height (μm)	n_{eff}
Meta-atom 1	2.7	0.6	1.6	1.3	5	20	2.3926
Meta-atom 2	3.0	0.6	1.6	1.5			2.7938
Meta-atom 3	2.9	0.6	1.7	1.5			2.9318
Meta-atom 4	2.7	0.6	2.9	1.5			3.6312

Optics EXPRESS

According to Eq. (7), we design an achromatic metalens with a diameter of 280 μm and a f-number of 1 aiming at the wavelength of 9~11 μm. The incident electromagnetic wave is left-handed circular polarization and the right-handed circularly polarized part of the transmitted field is focused. The cross-polarization equivalent refractive index, cross-polarization phase, and the required rotation angle at each radial coordinate across the achromatic metalens corresponding to the central wavelength are shown in Fig. 8(b)-(c), and the average cross-polarization transmission from 9 μm to 11 μm versus equivalent refractive index for different meta-atoms in our simulation library is shown in Fig. 8(a).

The model of the achromatic metalens is shown in Fig. 9(a). In order to validate the achromatic effect, we construct a diffractive metalens with the same aperture size and f-number based on

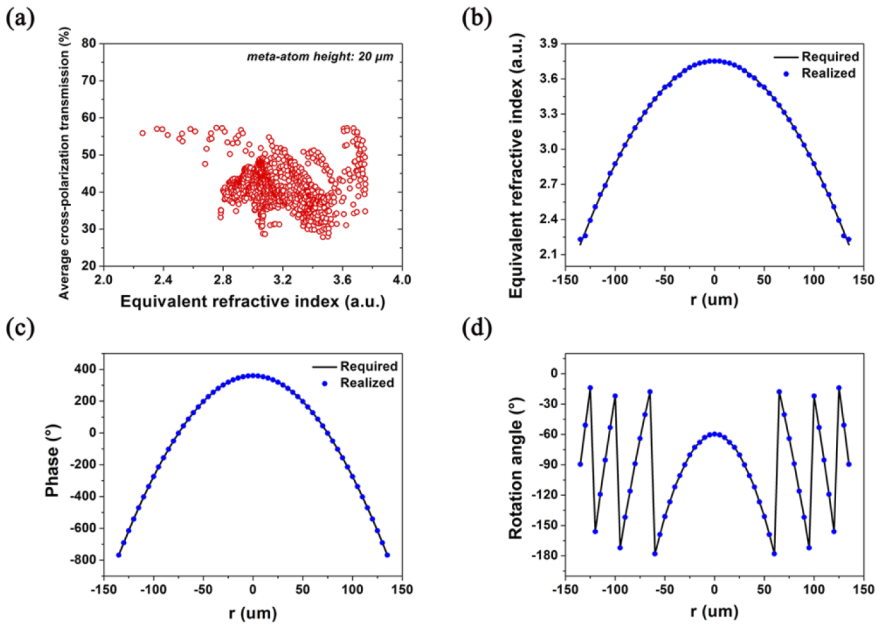

Fig. 8. (a) Average cross-polarization transmission from 9 μm to 11 μm versus equivalent refractive index for different meta-atoms in our simulation library. (b)-(c) Required and realized cross-polarization equivalent refractive index and phase at each radial coordinate across the achromatic metalens. (d) The rotation angle of the meta-atoms at each radial coordinate across the achromatic metalens.

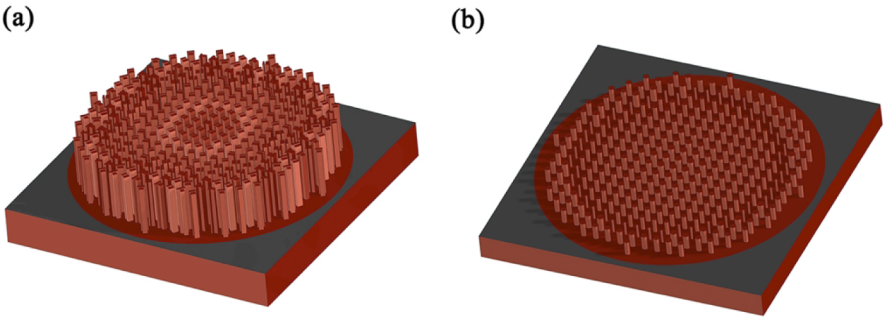

Fig. 9. (a) The schematic diagram of the achromatic metalens. (b) The schematic diagram of the diffractive metalens.

Optics EXPRESS

the selected elements in Fig. 2(b) to simulate the focusing property, as shown in Fig. 9(b). The material properties of these two metalenses are exactly the same.

In the comparative simulation of the metalens, we appropriately broaden the simulation wavelength range. It can be seen from the simulation results in Fig. 10, the achromatic metalens achieves good achromatic focusing effect from the wavelength of 8.6 to 11.4 μm, and the maximum focal length difference value in the working wavelength band is 5.5 μm. In contrast, the maximum focal length difference value of the diffractive metalens is 83 μm.

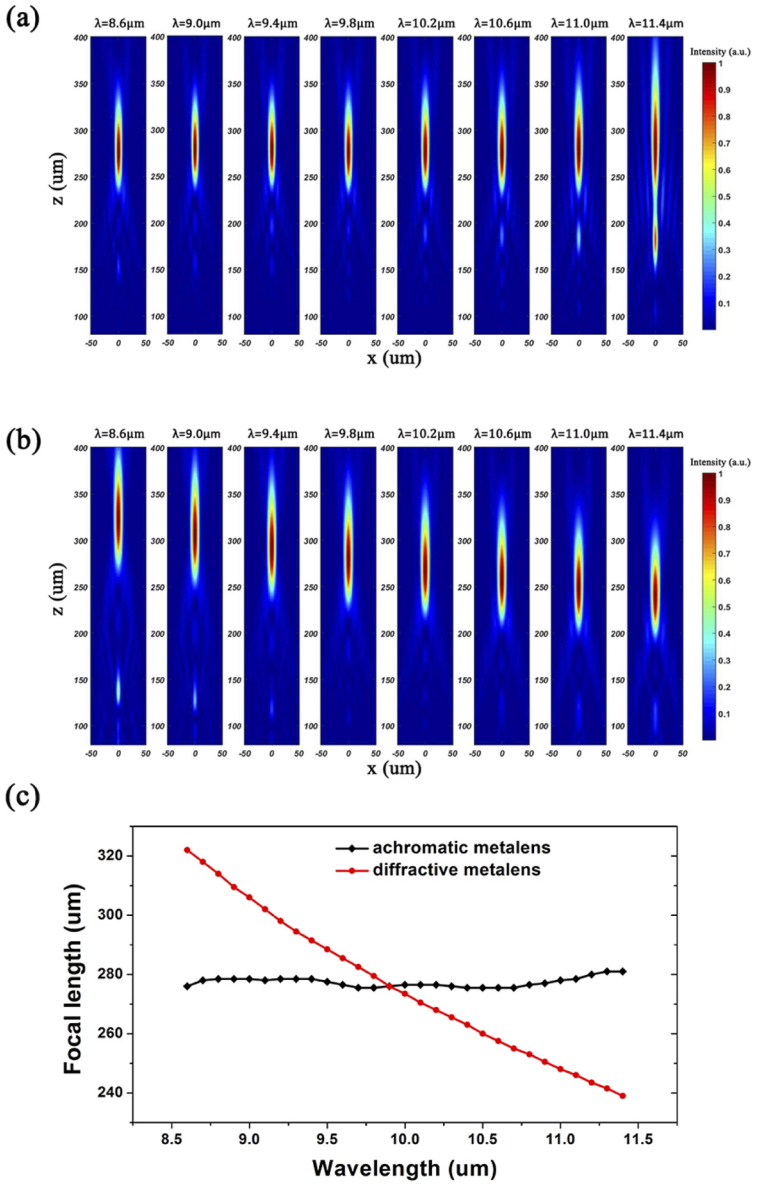

Fig. 10. (a) The focusing effect of the achromatic metalens from the wavelength of 8.6 to 11.4 μm. (b) The focusing effect of the diffractive metalens from the wavelength of 8.6 to 11.4 μm. (c) Comparison diagram of focal length of the two metalenses with wavelength.

Optics EXPRESS

Figure 11 shows the simulation results of the variation of the light intensity distribution with wavelength at the focal plane of the central wavelength. At this position, the focusing effect of the achromatic metalens in the wavelength range of 8.6–11.4 μm is close to the theoretical value of diffraction limit, while the focusing effect of the diffractive metalens at this position obviously changes with wavelength.

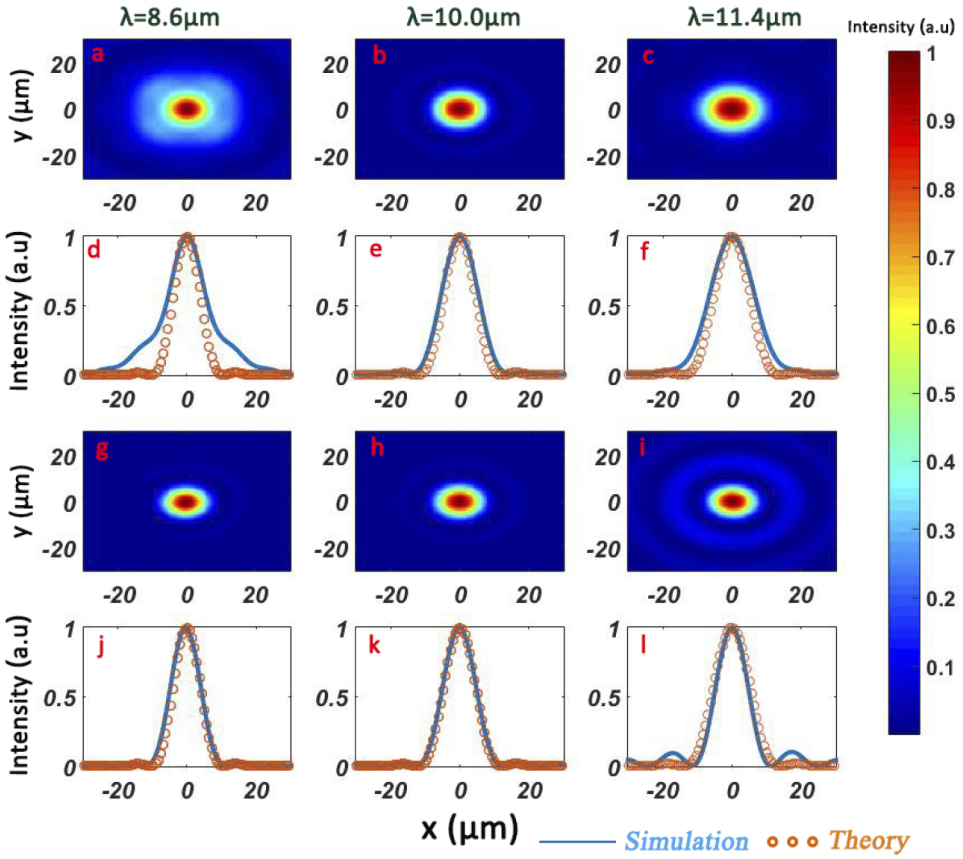

Fig. 11. (a)-(c) The two-dimensional variation diagram of the light intensity distribution of the diffractive metalens at different wavelength. (d)-(f) The one-dimensional variation diagram of the light intensity distribution of the diffractive metalens at different wavelength. (g)-(i) The two-dimensional variation diagram of the light intensity distribution of the achromatic metalens at different wavelength. (d)-(f) The one-dimensional variation diagram of the light intensity distribution of the achromatic metalens at different wavelength.

According to the Eq. (8), with the further optimization of deep silicon etching process, the aperture of the achromatic metalens is expected to further expand. Then, due to the limitation of the amount of the simulation work in this paper, the focusing efficiency of the achromatic metalens we designed is relatively low and the average value reaches 27.66% after eliminating the surface reflection of the unstructured surface, as shown in Fig. 12. The focusing efficiency of the achromatic metalens is expected to be improved by further expanding the parameters sweeping range and reducing the step value to obtain a larger parameters selection range.

Optics EXPRESS

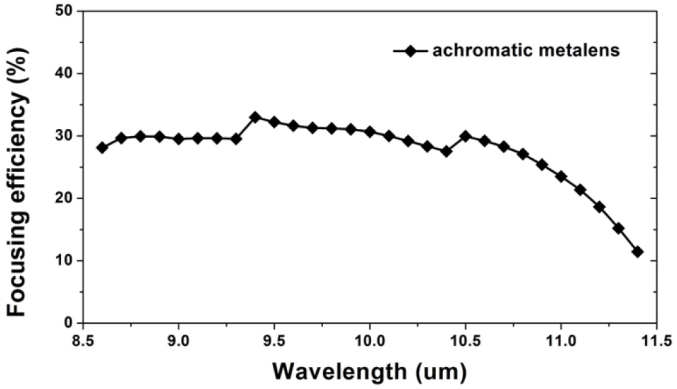

Fig. 12. The cross-polarization focusing efficiency of the designed achromatic metalens.

4. Conclusion

In summary, through introducing the fabrication characteristics of deep silicon etching into the design of the long-wavelength infrared achromatic metalens consisting of all-silicon meta-atoms with high aspect ratio, the imaging performance of the achromatic metalens can be further improved, and therefore the design possibility is extended. We have designed a silicon achromatic metalens whose aperture is 280 μm and f-number is 1, and the focusing effect close to the diffraction limit can be realized from the wavelength of 8.6 to 11.4 μm. The maximum focal length deviation percentage from the target value between the wavelength of 8.6 and 11.4 μm is 1.61% and the average focusing efficiency reaches 27.66%. In contrast, the maximum focal length deviation percentage of the diffractive metalens with the same aperture, the same material, and the same f-number is 15.0%. The achromatic metalens design strategy presented in this paper has certain maneuverability and is expected to play a role in the field of the LWIR integrated achromatic optics imaging system.

Funding. National Natural Science Foundation of China (61901437).

Disclosures. The authors declare no conflicts of interest.

Data availability. Data underlying the results presented in this paper are not publicly available at this time but may be obtained from the authors upon reasonable request.

References

1. M. Vollmer and K. P. Möllmann, *Infrared Thermal Imaging: Fundamentals, Research and Applications* (John Wiley & Sons, 2017).
2. M. Born and E. Wolf, *Principles of Optics: Electromagnetic Theory of Propagation, Interference and Diffraction of Light* (Elsevier, 2013).
3. W. T. Welford, *Aberrations of Optical Systems* (1st edition, Routledge, New York, 1986).
4. N. Yu, P. Genevet, M. A. Kats, F. Aieta, J.-P. Tetienne, F. Capasso, and Z. Gaburro, "Light propagation with phase discontinuities: generalized laws of reflection and refraction," Science **334**(6054), 333–337 (2011).
5. D. Lin, P. Fan, E. Hasman, and M. Brongersma, "Dielectric gradient metasurface optical elements," Science **345**(6194), 298–302 (2014).
6. P. Genevet, F. Capasso, F. Aieta, M. Khorasaninejad, and R. Devlin, "Recent advances in planar optics: from plasmonic to dielectric metasurfaces," Optica **4**(1), 139–152 (2017).
7. L. Huang, X. Chen, H. Muhlenbernd, G. Li, B. Bai, Q. Tan, G. Jin, T. Zentgraf, and S. Zhang, "Dispersionless phase discontinuities for controlling light propagation," Nano Lett. **12**(11), 5750–5755 (2012).
8. F. Aieta, M. A. Kats, P. Genevet, and F. Capasso, "Multiwavelength achromatic metasurfaces by dispersive phase compensation," Science **347**(6228), 1342–1345 (2015).
9. S. Sun, Q. He, S. Xiao, Q. Xu, X. Li, and L. Zhou, "Gradient-index meta-surfaces as a bridge linking propagating waves and surface waves," Nat. Mater. **11**(5), 426–431 (2012).

Optics EXPRESS

10. R. Paniagua-Dominguez, Y. F. Yu, E. Khaidarov, S. Choi, V. Leong, R. M. Bakker, X. Liang, Y. H. Fu, V. Valuckas, L. A. Krivitsky, and A. I. Kuznetsov, "A metalens with a near-unity numerical aperture," Nano Lett. **18**(3), 2124–2132 (2018).
11. K. Chen, Y. Feng, F. Monticone, J. Zhao, B. Zhu, T. Jiang, L. Zhang, Y. Kim, X. Ding, S. Zhang, A. Alù, and C.-W. Qiu, "A reconfigurable active huygens' metalens," Adv. Mater. **29**(17), 1606422 (2017).
12. J. Xiang, J. Li, H. Li, C. Zhang, Q. Dai, S. Tie, and S. Lan, "Polarization beam splitters, converters and analyzers based on a metasurface composed of regularly arranged silicon nanospheres with controllable coupling strength," Opt. Express **24**(11), 11420–11434 (2016).
13. S. An, B. Zheng, H. Tang, M. Y. Shalaginov, L. Zhou, H. Li, M. Kang, K. A. Richardson, T. Gu, J. Hu, C. Fowler, and H. Zhang, "Multifunctional metasurface design with a generative adversarial network," Adv. Opt. Mater. **9**(5), 2001433 (2021).
14. G. Zheng, H. Mühlenbernd, M. Kenney, G. Li, T. Zentgraf, and S. Zhang, "Metasurface holograms reaching 80% efficiency," Nat. Nanotechnol. **10**(4), 308–312 (2015).
15. X. J. Ni, A. V. Kildishev, and V. M. Shalaev, "Metasurface holograms for visible light," Nat. Commun. **4**(1), 2807 (2013).
16. S. Ge, P. Chen, Z. Shen, W. Sun, X. Wang, W. Hu, Y. Zhang, and Y. Lu, "Terahertz vortex beam generator based on a photopatterned large birefringence liquid crystal," Opt. Express **25**(11), 12349–12356 (2017).
17. Y. S. Rumala, G. Milione, T. A. Nguyen, S. Pratavieira, Z. Hossain, D. Nolan, S. Slussarenko, E. Karimi, L. Marrucci, and R. R. Alfano, "Tunable supercontinuum light vector vortex beam generator using a q-plate," Opt. Lett. **38**(23), 5083–5086 (2013).
18. S. Banerji, M. Meem, A. Majumder, F. G. Vasquez, B. Sensale-Rodriguez, and R. Menon, "Imaging with flat optics: metalenses or diffractive lenses?" Optica **6**(6), 805–810 (2019).
19. S. Wang, P. C. Wu, V.-C. Su, Y.-C. Lai, M.-K. Chen, H. Y. Kuo, B. H. Chen, Y. H. Chen, T.-T. Huang, J.-H. Wang, R.-M. Lin, C.-H. Kuan, T. Li, Z. Wang, S. Zhu, and D. P. Tsai, "A broadband achromatic metalens in the visible," Nat. Nanotechnol. **13**(3), 227–232 (2018).
20. W. T. Chen, A. Y. Zhu, V. Sanjeev, M. Khorasaninejad, Z. Shi, E. Lee, and F. Capasso, "A broadband achromatic metalens for focusing and imaging in the visible," Nat. Nanotechnol. **13**(3), 220–226 (2018).
21. R. J. Lin, V. Su, S. Wang, M. K. Chen, T. L. Chung, Y. H. Chen, H. Y. Kuo, J. Chen, J. Chen, Y. Huang, J. Wang, C. H. Chum P, C. Wu, T. Li, Z. Wang, S. Zhu, and D. P. Tsai, "Achromatic metalens array for full-colour light-field imaging," Nat. Nanotechnol. **14**(3), 227–231 (2019).
22. S. Wang, P. C. Wu, V. C. Su, Y. C. Lai, C. H. Chu, J. W. Chen, S. H. Lu, J. Chen, B. Xu, C. H. Kuan, T. Li, S. Zhu, and D. P. Tsai, "Broadband achromatic optical metasurface devices," Nat. Commun. **8**(1), 1–9 (2017).
23. J. Engelberg and U. Levy, "Optimizing the spectral range of diffractive metalenses for polychromatic imaging applications," Opt. Express **25**(18), 21637–21651 (2017).
24. Q. Fan, M. Liu, C. Yang, L. Yu, F. Yan, and T. Xu, "A high numerical aperture, polarization-insensitive metalens for long-wavelength infrared imaging," Appl. Phys. Lett. **113**(20), 201104 (2018).
25. Q. Fan, Y. Wang, M. Liu, and T. Xu, "High-efficiency, linear-polarization-multiplexing metalens for long-wavelength infrared light," Opt. Lett. **43**(24), 6005–6008 (2018).
26. M. Liu, Q. Fan, L. Yu, and T. Xu, "Polarization-independent infrared micro-lens array based on all-silicon metasurfaces," Opt. Express **27**(8), 10738–10744 (2019).
27. M. Khorasaninejad, A. Zhu, C. Roques-Carmes, W. T. Chen, J. Oh, I. Mishra, R. C. Devlin, and F. Capasso, "Polarization-insensitive metalenses at visible wavelengths," Nano Lett. **16**(11), 7229–7234 (2016).
28. G. J. Swanson, "Binary optics technology: the theory and design of multi-level diffractive optical elements," *Tech. Rep. 854, DTIC Document* (MIT Lincoln Laboratory, 1989).
29. M. J. Weber, *Handbook of Optical Materials* (CRC, 2018).
30. M. N. Vesperinas, *Scattering and Diffraction in Physical Optics* (2nd edition, World Scientific, Singapore, 2006).
31. H. Jansen, H. Gardeniers, M. de Boer, M. Elwenspoek, and J. Fluitman, "A survey on the reactive ion etching of silicon in microtechnology," J. Micromech. Microeng. **6**(1), 14–28 (1996).
32. M. Mao, Y. Wang, and A. Bogaerts, "Numerical study of the plasma chemistry in inductively coupled SF6 and SF6/Ar plasmas used for deep silicon etching applications," J. Phys. D: Appl. Phys. **44**(43), 435202 (2011).
33. S. Mas, J. Caraquitena, J. V. Galán, P. Sanchis, and J. Martí, "Tailoring the dispersion behavior of silicon nanophotonic slot waveguides," Opt. Express **18**(20), 20839–20844 (2010).
34. Y. Zhang, H. Liu, Q. Sun, N. Huang, and Z. Wang, "Supercontinuum generation in strip/slot hybrid waveguide with flat and low dispersion," Appl. Opt. **54**(15), 4850–4856 (2015).
35. M. Zhu, H. Liu, X. Li, N. Huang, Q. Sun, J. Wen, and Z. Wang, "Ultrabroadband flat dispersion tailoring of dual-slot silicon waveguides," Opt. Express **20**(14), 15899–15907 (2012).
36. Q. Chen, Y. Li, Y. Han, D. Deng, D. Yang, Y. Zhang, Y. Liu, and J. Gao, "High numerical aperture multifocal metalens based on Pancharatnam–Berry phase optical elements," Appl. Opt. **57**(27), 7891–7894 (2018).
37. W. Luo, S. Xiao, Q. He, S. Sun, and L. Zhou, "Photonic spin Hall effect with nearly 100% efficiency," Adv. Opt. Mater. **3**(8), 1102–1108 (2015).
38. J. Chen, F. Zhang, Q. Li, J. Wu, and L. Wu, "A high-efficiency dual-wavelength achromatic metalens based on Pancharatnam-Berry phase manipulation," Opt. Express **26**(26), 34919–34927 (2018).

Optics EXPRESS

39. X. Ding, F. Monticone, K. Zhang, L. Zhang, D. Gao, S. N. Burokur, A. de Lustrac, Q. Wu, C. W. Qiu, and A. Alù, "Ultrathin Pancharatnam-Berry metasurface with maximal cross-polarization efficiency," Adv. Mater. **27**(7), 1195–1200 (2015).
40. N. Yu and F. Capasso, "Flat optics with designer metasurfaces," Nat. Mater. **13**(2), 139–150 (2014).